Dents with Cracks that Shouldn't be, a Review of Failure Strain

Duncan Wang[1], Rhett Dotson[1], Rick Wang[2], Liam Hagel[2], Jing Wang[2]
[1]D2 Integrity, [2]TC Energy

Organized by

https://doi.org/10.52202/078572-0069

https://doi.org/10.52202/078572-0069

Abstract

In the Level-3 assessment of dents, the numerical results (e.g., stresses and plastic strains) from finite element analysis (FEA) were used to assess damage presence using two primary indices: the Ductile Failure Damage Indicator (DFDI) and the Strain Limit Damage (SLD). A pipeline dent is classified as damaged if either index exceeds unity. Both indices are derived from Rice and Tracey's micromechanics model, where void growth is influenced by plastic strain and stress triaxiality. However, recent studies have highlighted limitations in the failure strain formulations employed in these assessments. Specifically, research suggests that the scaling factor in the failure strain equation, initially set at 1.5, can be non-conservative, and experimental findings support higher values, such as 2.5. Additionally, concerns regarding void interactions and material-specific behaviour necessitate refinements in the current methodologies.

This study systematically reviews existing failure strain models used in DFDI and SLD evaluations and provides recommendations to address identified limitations. A continuous case study of two pipeline dents with metal loss and crack interactions demonstrates that previous Level-3 assessments failed to identify these anomalies. Through refined FEA assessments incorporating an updated failure strain approach, the injured dents were successfully flagged. The revised methodologies incorporate an upper-bound DFDI approach using a scaling factor of 2.5 and an improved SLD formulation that shifts the triaxiality anchor point to reflect worst-case material behaviours.

The findings underscore the importance of employing lower-bound failure strain approaches when material properties are uncertain, ensuring a more conservative evaluation of dent integrity. Key recommendations include adopting revised failure strain equations for both DFDI and SLD, prioritizing DFDI over SLD in dent assessments, and encouraging further experimental validation to refine failure strain parameters for pipeline steels. These refinements enhance the predictive capability of strain-based dent evaluations, reducing the risk of undetected damage in pipeline integrity assessments.

1. Introduction

The evaluation of pipeline dents is conducted at three levels, with this study concentrating on Level-3 assessment through finite element analysis (FEA). This sophisticated analysis assesses whether damage is present by utilizing two primary indices: the Ductile Failure Damage Indicator (DFDI) and the Strain Limit Damage (SLD). A pipeline dent is classified as damaged if the DFDI or SLD exceeds unity. Both indices were developed from Rice and Tracery's classic micromechanics model (i.e., a spherical void in a homogenous material), where the growth rate of the void depends on plastic strain levels and triaxial stress states. In DFDI and SLD, the damage indicator (D) was defined as the integration of damage increment ($d(D)$), where $d(D)$ is the ratio of the increment of equivalent plastic strain ($d(\varepsilon_{peeq})$) and failure strain (ε_f), i.e., $d(D) = d(\varepsilon_{peeq})/\varepsilon_f$. The equivalent plastic

https://doi.org/10.52202/078572-0069

strain is obtained from FEA, and ε_f depends on the material properties, where the failure strain was defined differently in DFDI and SLD. API 1183 provides recommended approaches for calculating the DFDI and SLD failure strains based on numerical analysis. Note that although most published studies (e.g., [1], [2], [3]) showed that fracture initiation could be identified on injured dents using DFDI or SLD, there are cases that failed to capture the presence of crack anomalies. That could be caused by the limits and gaps in the strain-based dent assessment [4]. For example, a previous study [5] reported that a number of dents were identified to interact with crack anomalies in the field assessment, but these incidents failed to be identified in the Level-3 assessment.

Several recent studies pointed out the limits of these recommended approaches in the failure strain. For the DFDI failure strain, Chae and Koss [6] pointed out that Rice and Tracery's study [7] did not consider void interactions, where voids are not isolated in a real material. When multiple voids are present, they interact with each other through stress fields. This interaction increases the overall void growth rate because neighbouring voids influence each other, creating stress concentration zones that amplify growth. Chae and Koss [6] also found that the scaling factor of the triaxiality term in failure strain formulation can be as high as 2.5 rather than 1.5 in Rice and Tracery's model based on experimental observations. Similarly, Yamada and Ohata [8] recently reported the scaling factor depends on the steel grade and is about 2.33 for HT780.

Li and Xi [1] examined the accuracy and applicability of the failure strain formulations defined in ASME BVPC Section VIII, Div 2, Part 5 for the SLD evaluation. Their study revealed that the ASME BPVC approach captures the upper bound strain limits; therefore, it is non-conservative overall for identifying the local fracture damage. In addition, Wang and Zhang [4] also pointed out the potential issues of DFDI calculations due to the strong dependence of failure strain on triaxiality when it ranges from 0.3 to 0.4 for pipe steel.

This study revisited the definitions of failure strains used in DFDI and SLD assessment to uncover related factors that may have contributed to the local fracture initiation. Based on this systematic review, recommendations are provided for failure strain assessment to assist operators and analysts in recognizing similar issues in the future. A case study was also conducted based on two recent field investigations where cracks near restrained dents were identified during excavation. It is a continuous investigation of cases reported in [5]. To the authors' best knowledge, the two injured dents failed to be flagged in the previous Level-3 assessment, as strain levels and damage indicators remained below critical thresholds.

From the comprehensive review of all the failure strain approaches related to DFDI and SLD calculations, the authors provided recommended formulations to eliminate or reduce the non-conservatism in predicting the local damage and fracture initiation. For example, the lower bound failure strain approach, which refers to the upper bound DFDI/SLD, should be employed if limited material information is available. The upper bound DFDI included a higher scaling factor of stress triaxiality ratio, 2.5, in the failure strain formulation. The upper bound SLD used a new anchor point

https://doi.org/10.52202/078572-0069

of stress triaxiality ratio (η_0) instead of 1/3 in the failure strain formulation. The case study results show that the recommended failure strain approach (i.e., upper bound and lower bound DFDIs/SLDs) can help add safety margins (i.e., reducing non-conservatisms) and identify the injured dent with some modifications.

2. Failure Strain: A Key Parameter

Failure strain (ε_f) is a critical factor in assessing whether microvolumes in a material have sustained damage, mainly the state of fracture initiation. It forms the foundation of strain-based damage indicators (D):

$$D = \int d\left(\frac{\varepsilon_{peeq}}{\varepsilon_f}\right) \quad \text{Eq. (1)}$$

where ε_{peeq} is the effective plastic strain[1], and $D \geq 1$ indicates damage, i.e., the fracture initiation. In the past five decades, a pronounced number of theoretical and experimental studies have been conducted on the failure strain. McClintock [9] first investigated cylindrical voids and introduced the concept of failure strain. Later, several analytical models were developed, which are either phenomenological based or plasticity theory-based. The phenomenological-based models are mainly based on experimental or numerical analyses, e.g., Johnson and Cook [10]. The parameters in the phenomenological models are empirically based and may not have direct physical meaning. They are obtained or calibrated by performing nonlinear regression analysis on the experimental data. On the other hand, the plasticity theory-based models were derived from continuum mechanics in the micro-scale model, e.g., McClintock [9] and Gurson-Tvergaard-Needleman (GTN) model [11]. The parameters of the models have physical meaning, and therefore, they can be determined from theoretical calculations and/or experimental calibrations. A two-parameter general form of void growth-based failure strain is widely used and defined as

$$\varepsilon_f = a\exp\left(-b\eta\right) \quad \text{Eq. (2)}$$

where a is the material property, b is the scaling factor, and η the stress triaxiality ratio. Note that the form of Eq. (2) was initially proposed by Rice and Tracey [7].

For the engineering critical assessment (ECA) of dents, the recommended practice of API 1183 employed two damage indices: DFDI and SLD. Both are defined in the form of Eq. (1), where ε_f has different definitions. The DFDI's ε_f is from the plasticity theory model [7], and the SLD's ε_f has a hybrid form (phenomenological and plasticity theory-based) presented in ASME BPVC Section VIII, Division 2, Part 5 [12].

2.1. DFDI's Failure Strain

The failure strain of DFDI is defined as

[1] PEEQ is an Abaqus® term and represents **P**lastic **S**train **EQ**uivalent.

https://doi.org/10.52202/078572-0069

$$\varepsilon_f = 1.65\varepsilon_0 \exp(-1.5\eta) \quad \text{Eq. (3)}$$

where η is the stress triaxiality ratio, and ε_0 is the critical strain at the uniaxial stress state. The stress triaxiality ratio is defined as

$$\eta = \frac{\sigma_m}{\sigma_{eq}} \quad \text{Eq. (4)}$$

where σ_m is the hydrostatic stress, and σ_{eq} is the von Mises equivalent stress. API 1183 [13] recommends using the upper and lower bound of failure strains for DFDI calculation based on uniaxial and biaxial stress states, where

- $DFDI_{lower\ bound}$ – uniaxial stress state ($\eta = 1/3$) : $\varepsilon_f = \varepsilon_0$
- $DFDI_{upper\ bound}$ – biaxial stress state ($\eta = 2/3$): $\varepsilon_f = \frac{\varepsilon_0}{1.65}$

2.1.1. Background of DFDI's Failure Strain

Eq. (3) was developed from Eq. (2) where the growth and shape change of a spherical void in a homogenous matrix were considered [7]. Rice and Tracey's model demonstrated that the void growth depends exponentially on triaxial stress states, and the failure strain was defined as

$$\varepsilon_f = 0.283 \exp(-1.5\eta) \quad \text{Eq. (6)}$$

In Hancock and Mackenzie's study (see Eq. (13) in [14]), the failure strain is expressed as

$$\varepsilon_f = a \exp(-1.5\eta) \quad \text{Eq. (7)}$$

where a is a material constant. Later, Fischer et al. [15] proposed the revised Eq. (7), i.e., Eq. (3), based on the investigations of a spherical void in a triaxial principal stress field. Fischer et al. [15] also found that the material constant $a \approx 1.65\varepsilon_0$, which is calculated from the uniaxial stress state ($\eta = 1/3$ and $\varepsilon_f = \varepsilon_0$):

$$\varepsilon_f/\varepsilon_0 = a \exp(-1.5\eta)/\varepsilon_0 = a \exp\left(-1.5 * \frac{1}{3}\right)/\varepsilon_0 = a \exp\left(-\frac{1}{2}\right)/\varepsilon_0 = 1 \quad \text{Eq. (8)}$$

$$a \approx 1.65\varepsilon_0 \quad \text{Eq. (9)}$$

The detailed procedures to calibrate the critical strain ε_0 was presented in Section 3 of [15]. Later, Gao et al. [2] provided the details regarding how to use dog bone coupons to calibrate ε_0 for pipeline steels. Fischer's work [15] formed the basis of current DFDI and related failure strain approach. It should be noted that Eqs. (3), (6) and (7) have the same scaling factor, i.e. $b = 1.5$. That is mainly because all these equations were developed by treating the void as an isolated sphere, and they did not consider the interactions between adjacent voids.

2.1.2. Recent Development of Rice-Tracey's Model-Based Failure Strain

A recent study by Chae and Koss [6] considered the interaction between adjacent voids and compared fractographic data with Rice and Tracey's model. The experimental results indicated the stress triaxiality scaling factor of 2.5 should be considered rather than 1.5 for HSLA-100 steel. In addition, Chae and Koss [6] reported the material constant is about 0.58, i.e., $1.65\varepsilon_0 = 0.58$, which makes $\varepsilon_0 \approx 0.35$. It is close to the lower bound value of 0.3 recommended in API 1183, and it is less than

https://doi.org/10.52202/078572-0069

the theoretical value of 0.85 reported by Huang [16] ($\varepsilon_0 \approx 0.50$). Yamada and Ohata [8] reported that the scaling factor should be 2.33 for HT780 steel based on experimental and numerical studies. Besides the above-mentioned quantitative studies on the failure strain, there is a pronounced number of research on qualitative investigations on the failure strain, e.g., [10], [17], [18], [19], [20], [21]. Johnson and Cook [10] investigated failure strain for three metals. They pointed out that the scaling factor of stress triaxiality is a material-specific constant, indicating variability in the scaling factor across different metals. Xue and Wierzbicki [18] revisited their experimental data. They found that all the failure strains were bounded by two lines (upper bound and lower bound) corresponding to the axisymmetric stress state and plane strain state, see Fig.1. Later, Bao and Wierzbicki [22] presented experimental and numerical analyses on 2024-T351 Aluminium alloy and demonstrated that the scaling factor is not constant but rather depends on the loading conditions. Experimental results in Barsoum and Faleskog's paper [19] show that the failure strain for Weldox 420 and Weldox 960 steel varies with stress triaxiality, suggesting that the scaling factor deviates from 1.5 under different loading conditions.

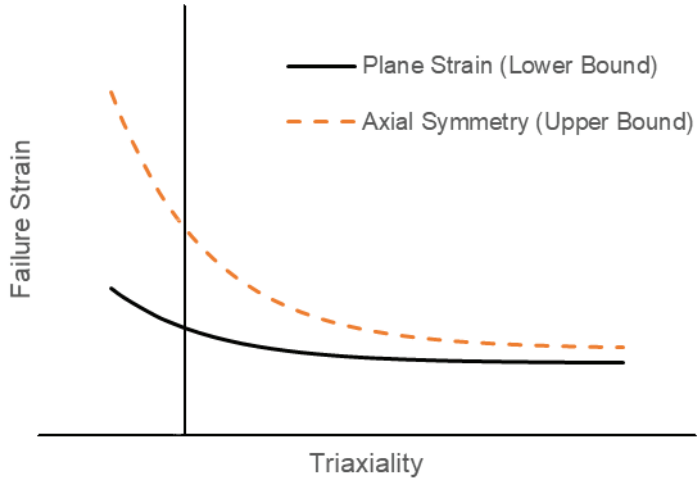

Figure 1: Schematic Plots of Upper Bound of Failure Strain (Axisymmetric Stress State) and Lower Bound of Failure Strain (Plane Strain State) from Xue and Wierzbicki's Material Ductility Report [18].

2.1.3. Impact of Failure Strain on DFDI Assessment

Section 2.1.2. presented that the recent studies on the failure strain assessment, and one of the key findings was the scaling factor of stress triaxiality (i.e., coefficient 1.5 in Eq. (3) or parameter b in Eq. (10)) is not a constant. The factors depend on material properties and the triaxial stress state. Among all the literature, the maximum and minimum scaling factors reported are 2.5 and 1.5, respectively. The values of $b = 2.5$ and $b = 1.5$ were developed from models with and without void interactions, respectively. The presence of void interactions may be caused by closely spaced voids (e.g., those near coalescence or cluster voids), which can accelerate the void growth with an increased stress triaxiality

https://doi.org/10.52202/078572-0069

ratio. Figure 2 shows the failure strain calculated from Eq. (3) with two scaling factors, i.e. $b = 2.5$ and $b = 1.5$, where the critical strain $\varepsilon_0 = 0.3$ is assumed per API 1183 [13]. The figure shows that the failure strain decreases with the increase of the scaling factor. The difference of failure strains is calculated from the following equation and shown in Fig. 2.

$$Diff = \frac{\varepsilon_{f,1.5} - \varepsilon_{f,2.5}}{\varepsilon_{f,2.5}} \quad \text{Eq. (11)}$$

where $\varepsilon_{f,1.5}$ and $\varepsilon_{f,2.5}$ are values calculated from $b = 1.5$ and $b = 2.5$, respectively. Results in Fig. 2 show that the failure strain can be overestimated by about 40-100% within the interested triaxiality $(1/3 \leq \eta \leq 2/3)$ for dent ECAs, i.e., between uniaxial and biaxial stress states.

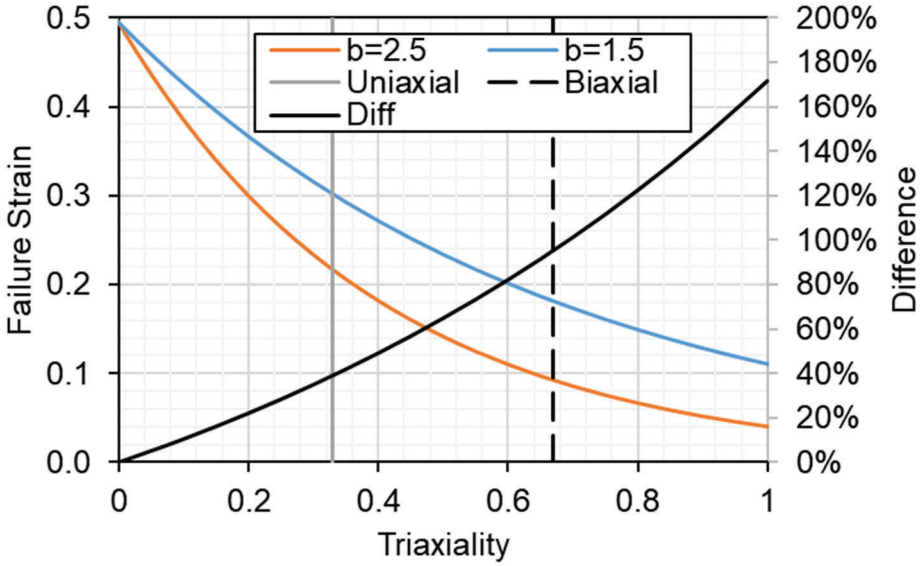

Figure 2: Failure Strains from Scaling Factor b=1.5 and 2.5, and Difference of Calculated Failure Strains.

Using different scaling factors will result in different failure strains and, then, different DFDI values. Figure 3 shows the calculated DFDI values at different plastic strain levels (i.e., PEEQ = 5%, 10%, 15%, and 20%) using two stress triaxiality scaling factors ($b = 1.5$ and 2.5). Note that the figure shows the mathematical relations between DFDI and PEEQ/Triaxiality rather than a look-up datasheet. The results show the following observations:

(1) DFDI values gradually increase with stress triaxiality, and
(2) differences in DFDI values at $b = 1.5$ and 2.5 rapidly increase with the increase of PEEQ levels.

For example, at PEEQ =15%, DFDI values are less than the threshold value (i.e., DFDI < 1) if the scaling factor $b = 1.5$ (dashed green curve). On the other hand, DFDI values are greater than the threshold value (i.e., DFDI ≥ 1) at $\eta > 0.49$ if the scaling factor $b = 2.5$ (solid green curve). Note that the stress triaxiality state of 0.49 can be observed in the vicinity of the dent apex in the Level-3 assessment.

https://doi.org/10.52202/078572-0069

It is worth noting that the scaling factor of stress triaxiality directly impacts the calculated DFDI value, and the scaling factor depends on the stress/strain state (e.g. plane strain state) and material (e.g., type of material, with/without void interactions). For dent ECAs, if the pipe steel properties are not available (e.g., void type, void volume fraction, void cluster), the two stress triaxiality scaling factors, i.e., $b = 1.5$ and 2.5, should be considered in the failure strain and DFDI calculations.

$$\begin{cases} \varepsilon_f = 1.65\varepsilon_0 \exp(-1.5\eta), upper\ bound\ (i.e.,\ lower\ bound\ DFDI) \\ \varepsilon_f = 1.65\varepsilon_0 \exp(-2.5\eta), lower\ bound\ (i.e., upper\ bound\ DFDI) \end{cases} \quad \text{Eq. (12)}$$

Using the lower bound failure strain (i.e., upper bound DFDI) can reduce the non-conservatism in the DFDI evaluation. Note that (1) the scaling factor of 2.5 is the maximum value reported in the literature so far, and (2) the upper bound DFDI assessment mentioned here is different from that in API 1183 (bi-axial stress state).

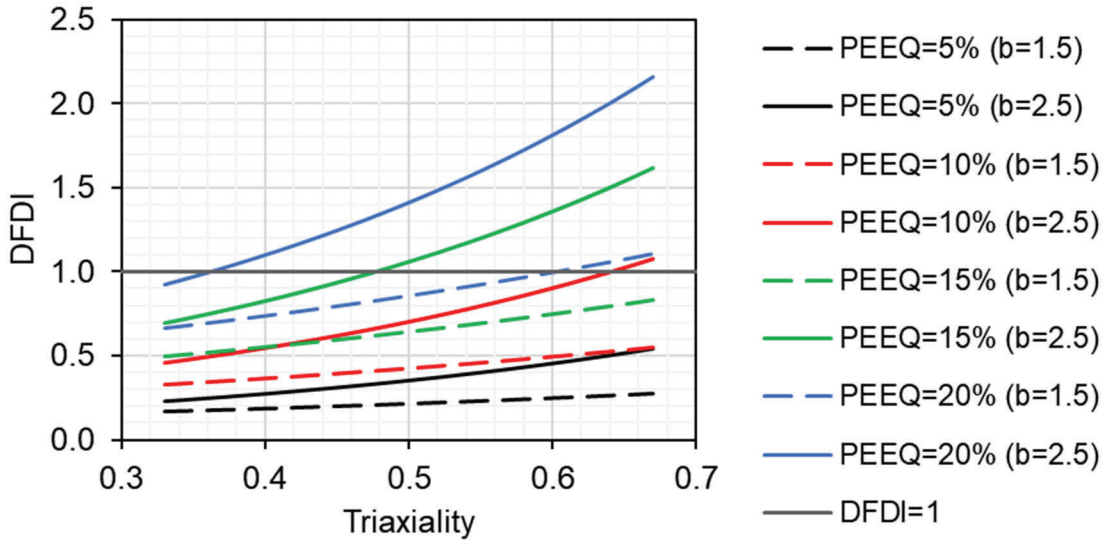

Figure 3: DFDI at Different PEEQ Levels Calculated from Scaling Factors of 1.5 and 2.5.

2.2. SLD's Failure Strain

The failure strain of SLD is defined in ASME BPVC Section VIII, Division 2, Part 5 [12].

$$\varepsilon_{L,k} = \varepsilon_{Lu}\left[\exp\left(-\frac{m_5}{1+m_2}\left(\eta_k - \frac{1}{3}\right)\right)\right] \quad \text{Eq. (13)}$$

where $\varepsilon_{L,k}$ is the failure strain at k_{th} loading step ($\varepsilon_{Lu} = max(m_2, m_3, m_4)$ per Section KD-232 of [12]), and $m_{2,3,4,5}$ are inputs from Table KD-230.5 and defined as follows:

$$m_2 = 0.60\left(1.00 - \frac{\sigma_{ys}}{\sigma_{uts}}\right) \quad \text{Eq. (14)}$$

$$m_3 = 2ln\left(1 + \left(\frac{El}{100}\right)\right) \quad \text{Eq. (15)}$$

$$m_4 = \ln\left(\frac{100}{100-RA}\right) \quad \text{Eq. (16)}$$

https://doi.org/10.52202/078572-0069

$$m_5 = 2.2 \text{ for pipe steel} \quad \text{Eq. (17)}$$

If the minimum specified reduction area (RA) is not available, ε_{Lu} is the maximum value of m_2 and m_3. Based on Table 6 of API 5L [23], the parameter m_3 is calculated based on the minimum specified elongation (El) using the following equation:

$$A_f = C\frac{A_{XC}^{0.2}}{U^{0.9}} \quad \text{Eq. (18)}$$

where A_f is the minimum specified elongation (El), $C = 625{,}000$ using the imperial unit, A_{XC} is the tensile coupon cross-section area per ASTM E8 [24], and U is the minimum tensile strength.

2.2.1. Background of SLD's Failure Strain

Prager and Osago [12] first proposed the SLD's failure strain (Eq. 13) after benchmarking a series of experimental studies. The predominant testing results were from Bridgeman's works on notch bars and tensile tests under ambient and high-pressure conditions, which considered different triaxial stress states after the post-necking state of ferritic and austenitic steel coupons.

Eq. (13) was obtained by solving the following equation at the uniaxial stress state ($\eta = 1/3$).

$$\varepsilon_{fm} = \sqrt[\frac{1}{1+m_2}]{\frac{1+m_2}{S_0\gamma}}\left[\exp\left(-\frac{m_5}{1+m_2}\eta\right)\right] \quad \text{Eq. (19)}$$

where ε_{fm} refers to the multi-axial failure strain, S_0 is the true stress level where the true strain equals unity, and γ is a material constant dependent on material properties (e.g., grain size, cleanliness, inclusion content, and 2nd phase particle size). At the uniaxial stress state, Eq. (19) becomes

$$\varepsilon_{fu} = \sqrt[\frac{1}{1+m_2}]{\frac{1+m_2}{S_0\gamma}}\left[\exp\left(-\frac{m_5}{1+m_2}*\frac{1}{3}\right)\right] \quad \text{Eq. (20)}$$

where ε_{fu} is the uniaxial failure strain. The ratio of multi-axial to uniaxial failure strains becomes

$$\frac{\varepsilon_{fm}}{\varepsilon_{fu}} = \frac{\sqrt[\frac{1}{1+m_2}]{\frac{1+m_2}{S_0\gamma}}\left[e^{-\frac{m_5}{1+m_2}\eta}\right]}{\sqrt[\frac{1}{1+m_2}]{\frac{1+m_2}{S_0\gamma}}\left[e^{-\frac{m_5}{1+m_2}*\frac{1}{3}}\right]} = \left[\exp\left(-\frac{m_5}{1+m_2}\left(\eta-\frac{1}{3}\right)\right)\right] \quad \text{Eq. (21)}$$

Based on the following two conditions, Eq. (21) can be solved, and Eq. (13) is obtained.

(1) Multi-axial limit strain equals multi-axial failure strain, $\varepsilon_{fm} = \varepsilon_{Lm}$

(2) Uniaxial limit strain equals uniaxial failure strain, $\varepsilon_{fu} = \varepsilon_{Lu}$

2.2.2. Recent Development of SLD's Failure Strain

Li and Xi [25] reviewed the accuracy and applicability of ASME-SLD's failure strain model and compared it against other local fracture models used in pressure vessel assessment. It was found that Eq. (13) – SLD's failure strain is not conservative overall, and the worst-case stress state is not uniaxial tension $\eta = 1/3$ but around $\eta = 0.16$ or $\eta = 0.50$. Note that $\eta = 0.50$ is close to the maximum stress triaxiality level at the dent damaged location.

https://doi.org/10.52202/078572-0069

Li and Xi [25] proposed a lower bound failure strain model (Eq. (22)) validated against experimental results of aluminium alloys and low to medium-carbon steels. The non-conservatism in the SLD calculation can be eliminated by using the lower bound failure strain from their study.

$$\varepsilon_{L,k} = \varepsilon_{Lu}\left[\exp\left(-\frac{m_5}{1+m_2}(\eta-\eta_0)\right)\right] \quad \text{Eq. (22)}$$

In Eq. (22), the anchor point of the stress triaxiality shifts from the uniaxial stress state $\eta = 1/3$ to the worst-case stress state η_0. The parameter η_0 is defined as

$$\eta_0 = \frac{1}{3(1-\alpha)}\left(3-\sqrt{(2+\alpha)^2+\frac{3\alpha^4}{(2-\alpha)^2}}\right) \quad \text{Eq. (23)}$$

where α is a function of material constants m_2, m_5:

$$\alpha = 4 - 3\exp\left(\frac{m_2 m_5}{3(m_2+1)}\right) \quad \text{Eq. (24)}$$

2.2.3. Impact of Failure Strain on SLD Assessment

Section 2.2.2. presented a recent study on the SLD's failure strain, and one of the key findings was that the current approach could lead to non-conservative predictions of local fracture initiation. That is mainly because the anchor point of the stress state was assumed to be the uniaxial tension state, where $\eta = 1/3$, rather than the worst-case stress state. The benchmarking studies showed that the worst-case state should be at $\eta = 0.16$ or $\eta = 0.50$. The revised form of failure strain was proposed to capture lower bound strain levels and eliminate non-conservatism in the damage assessment.

Figure 4 shows the failure strain calculated from Eq. (13) and Eq. (22) based on the material properties of API 5L's X52 pipe steel. The figure shows that the failure strain from the lower bound approach is about 27.5% less than that from ASME BPVC's approach at $1/3 \le \eta \le 2/3$. The use of lower bound failure strains will result in higher SLD values. Using two approaches, figure 5 shows the calculated SLD values at different plastic strain levels (i.e., PEEQ = 5%, 10%, 15%, and 20%). Note that the figure shows the mathematical relations between SLD and PEEQ/Triaxiality rather than a look-up datasheet. The results show that (1) SLD values gradually increase with stress triaxiality and (2) differences in SLD values from the two approaches rapidly increase with the increase of PEEQ levels.

It is worth noting that anchor points of stress state in failure strain calculations directly impact the calculated SLD value. Since the worst case of stress states may not be at uniaxial condition $\eta = 1/3$, it is recommended that the SLD assessment adopt Li and Xi's lower bound approach along with the current ASME BPVC approach (as upper bound). The use of the lower bound failure strain (i.e., upper bound SLD) can reduce the non-conservatism in the SLD assessment.

$$\begin{cases} \varepsilon_{L,k} = \varepsilon_{Lu}\left[\exp\left(-\frac{m_5}{1+m_2}\left(\eta_k-\frac{1}{3}\right)\right)\right], \textit{upper bound (i.e., lower bound SLD)} \\ \varepsilon_{L,k} = \varepsilon_{Lu}\left[\exp\left(-\frac{m_5}{1+m_2}(\eta-\eta_0)\right)\right], \textit{lower bound (i.e., upper bound SLD)} \end{cases} \quad \text{Eq. (25)}$$

https://doi.org/10.52202/078572-0069

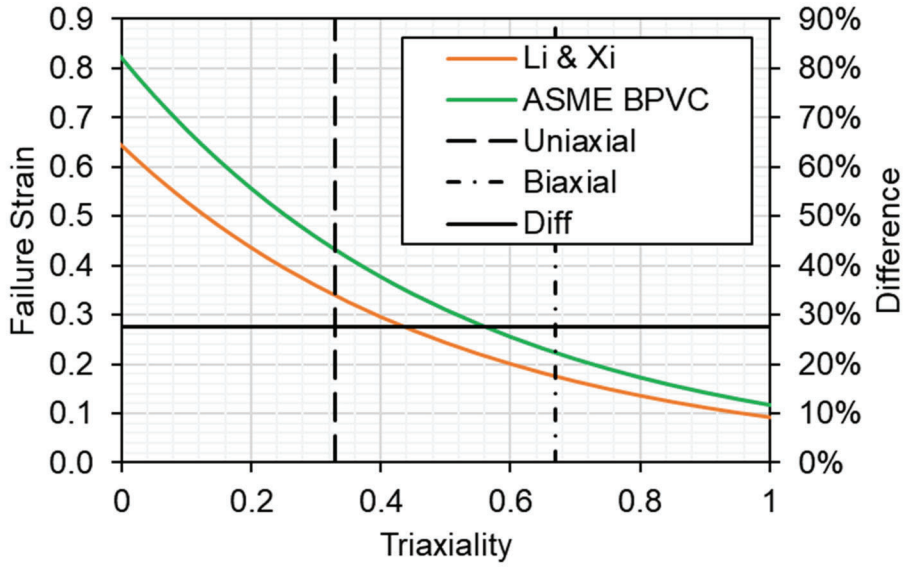

Figure 4: Failure strains from Eq.(13) and Eq. (23), and difference of calculated failure strains.

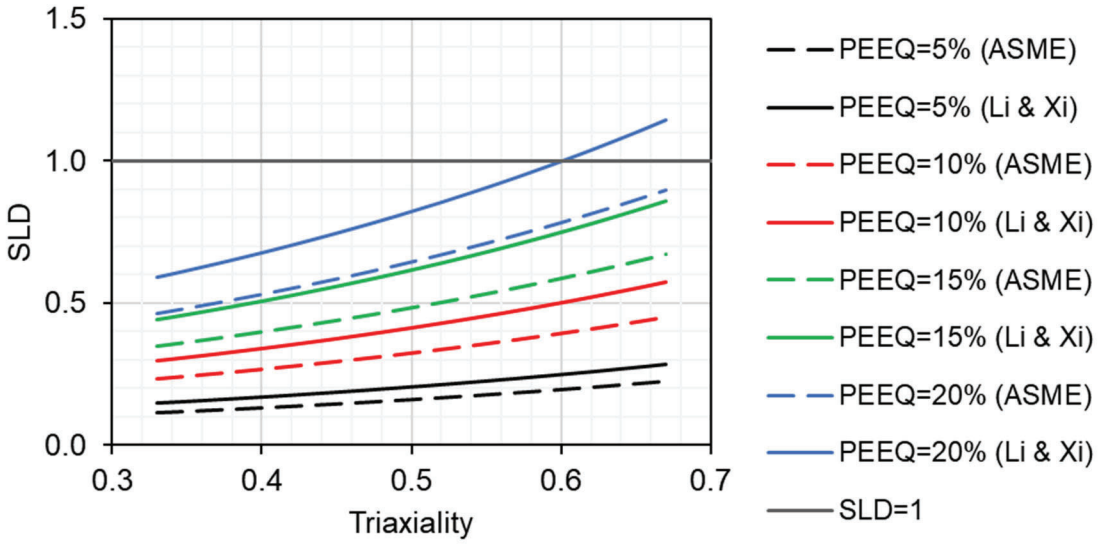

Figure 5: SLD at different PEEQ levels calculated from two failure strain approaches.

3. Case Studies

Two recent field assessments were used for the case studies to show the impact of failure strain approaches on the DFDI and SLD calculations for dents.

3.1. Finite Element Models

https://doi.org/10.52202/078572-0069

The finite element (FE) model used in this assessment consists of both shell and solid regions, and the shell-solid coupling technique was adopted for the shell and solid transition region. Second-order elements (C3D20 and S8R) were used to capture the mid-node curvature, which reduces any rigidity in bending caused by 1st order elements.

An example of an FE model is shown in Fig. 6. The detailed hexahedral solid elements in the vicinity of the dent feature are shown in Fig. 7. In total, there are six (6) layers of elements through wall thickness to capture the corresponding nonlinear variation of stress and strain at the dent. Based on the mesh sensitivity studies, a solid element size of 0.2 ~ 0.3 inch (i.e., 5 ~ 6 mm) is used for the analysis.

The metal loss feature was modelled to match the reported box area accounting for ILI tool tolerances. An additional safety margin was included when removing elements, which means all the elements interacting with projected areas were removed. An image of a simulated metal loss feature in the FE model is shown in Fig. 7.

Figure 6: Meshing of FE model.

https://doi.org/10.52202/078572-0069

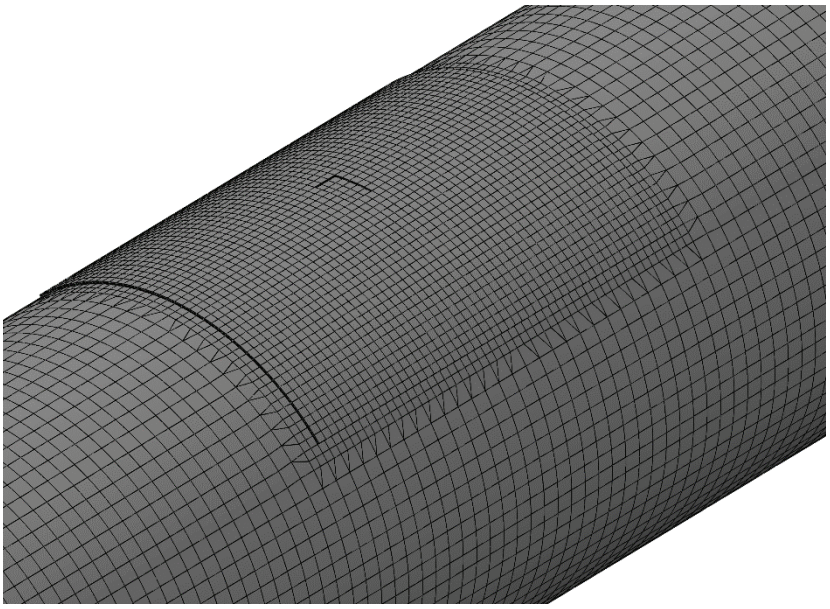

Figure 7: Meshing of solid element with metal loss

3.2. Material Model

The Ramberg-Osgood formulation was used to capture the true stress and true strain relationship in the FE model per API 579 [26].

$$\varepsilon_t = \varepsilon_e + \varepsilon_p = \frac{\sigma_t}{E_y} + \left(\frac{\sigma_t}{H_{RO}}\right)^{\frac{1}{n_{RO}}} \quad \text{Eq. (26)}$$

where ε_t, ε_e, and ε_p are true total strain, elastic strain, and plastic strain, respectively; σ_t refers to the true stress; E_y is the Young's modulus; n_{RO} and H_{RO} are defined as follows:

$$n_{RO} = \frac{1}{A_{RO}} \ln\left[\frac{\sigma_{uts}}{\sigma_{ys}}\right]^{B_{RO}} \quad \text{Eq. (27)}$$

$$H_{RO} = \frac{\sigma_{uts} \exp[n_{RO}]}{{n_{RO}}^{n_{RO}}} \quad \text{Eq. (28)}$$

where A_{RO} and B_{RO} are coefficients defined in API 579 [26]:

- Yield offset strain $\varepsilon_{ys} = 0.2\%$, $A_{RO} = 3.93$ and $B_{RO} = 0.754$;
- Yield offset strain $\varepsilon_{ys} = 0.5\%$, $A_{RO} = 3.27$ and $B_{RO} = 0.690$;

For example, by assuming the yield offset strain $\varepsilon_{ys} = 0.2\%$, the true stress and true strain curve for X52 pipe steel, is plotted in Fig. 8, where $\sigma_{ys} = 52{,}200\ psi$ and $\sigma_{uts} = 66{,}700\ psi$ per API 5L [27].

https://doi.org/10.52202/078572-0069

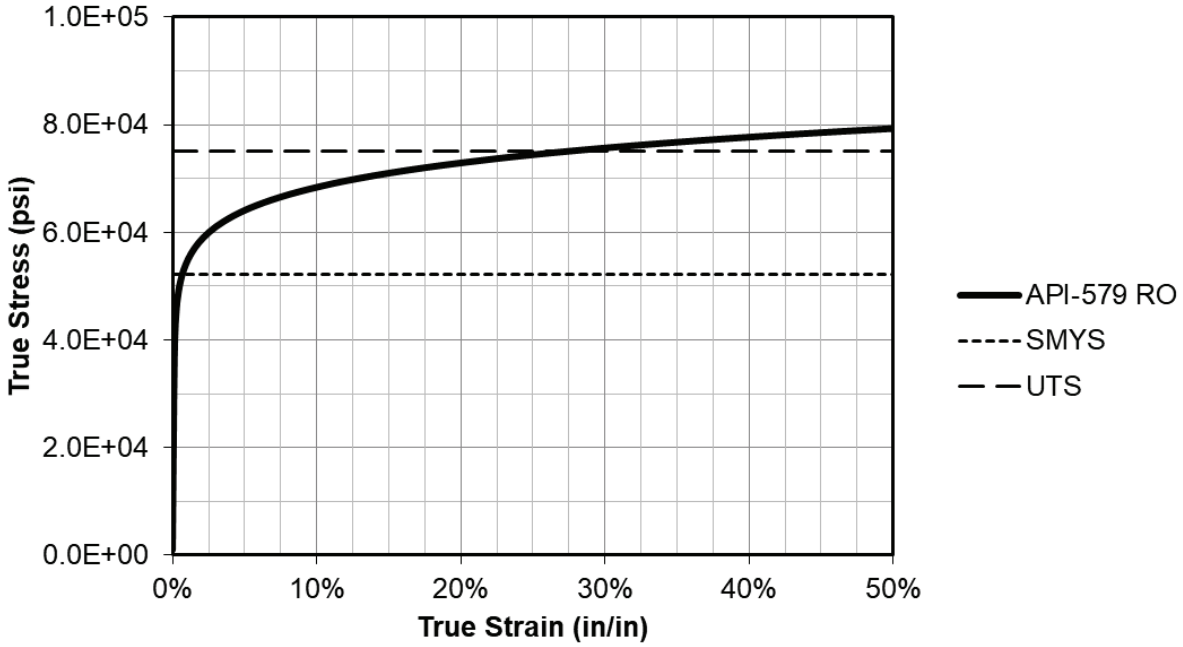

Figure 8: API 5L X52 true stress and true strain curve based on Ramberg-Osgood Model.

3.3. Field Investigations

The previous publication [5] identified two restrained dents reported as interacting with metal losses but were found to have cracks. The cracks are located near or at the dent apex in both cases. It is suspected that the cracks initiated at the ID on a metallurgical analysis. Figures 9 and 10 show the details of dent and crack interactions for two dents, i.e., DNT-1 and DNT-2.

The two dents are on a 26-inch diameter pipe with 0.281-inch wall thickness. The pipe is made from API 5L X52 carbon steel and contains an electric flash welded (EFW) longitudinal seam. Note that both dents were reported on the same line, with the same pipe manufacturer (A.O. Smith). The pipeline was installed in the 1960s. The maximum allowable operating pressure is 800 psig, corresponding to 71% of the specified minimum yield strength (SMYS). The most recent hydrostatic test was performed to a minimum pressure of 1,179 psig for DNT-1 and 964 psig for DNT-2. The most recent in-line inspection (ILI) was performed using an electromagnetic acoustic transducer (EMAT) tool, and no anomalies were identified at the location of interest.

The axial and circumferential profiles of two dents are shown in Figs. 11 and 12. The following section will present and compare the profiles from iterative FE simulations against the caliper-measured profiles.

https://doi.org/10.52202/078572-0069

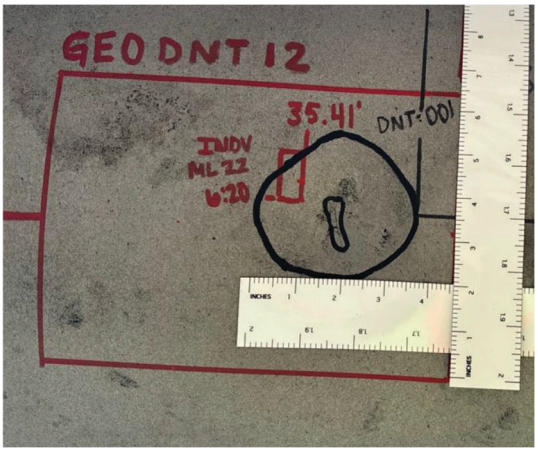

Dent with Metal Loss and Crack

Photo of Crack Taken from OD

Figure 9: DNT-1 with metal loss and crack.

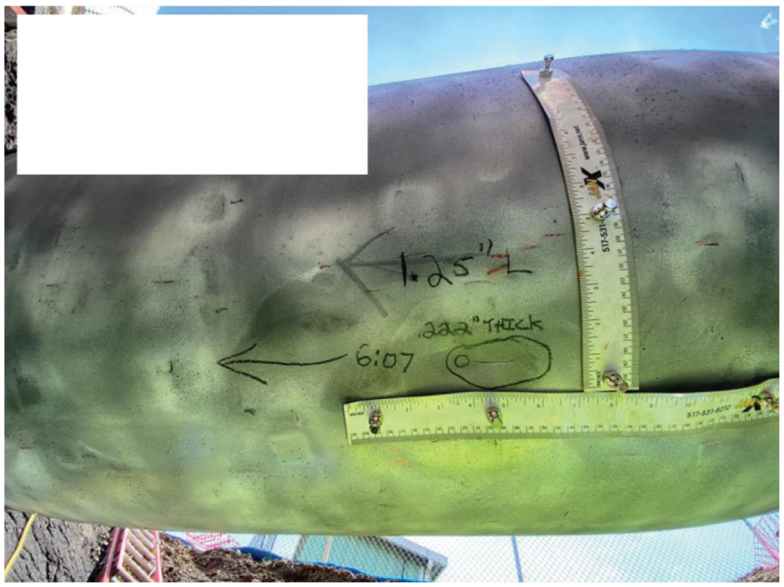

Figure 10: DNT-2 with metal loss and crack

https://doi.org/10.52202/078572-0069

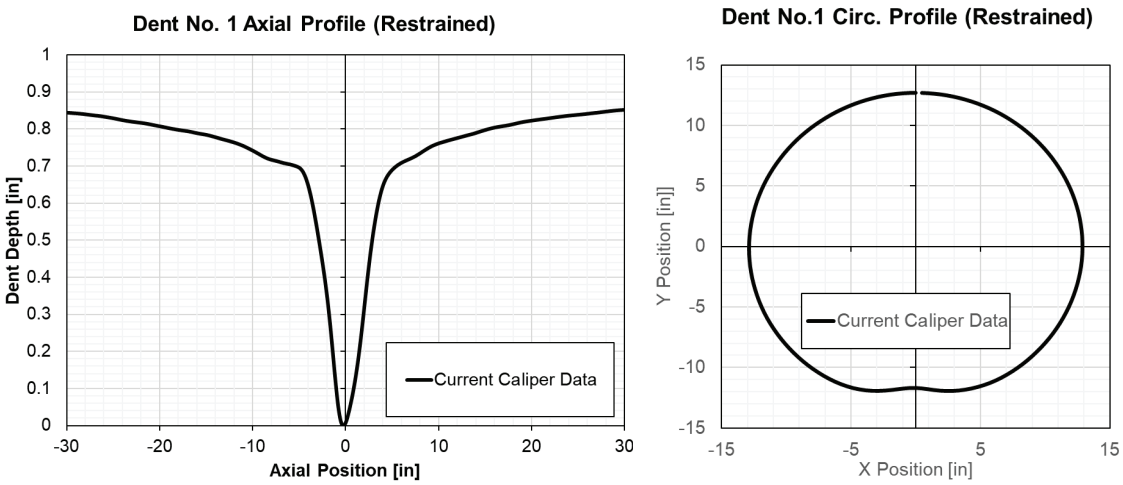

(a) Axial profile (b) Circumferential profile

Figure 11: Axial and circumferential profiles of DNT-1

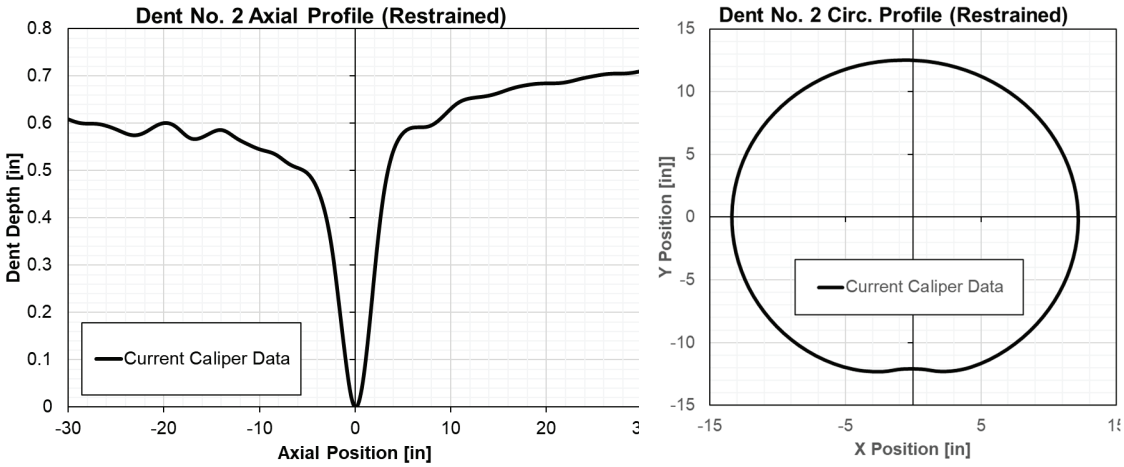

(a) Axial profile (b) Circumferential profile

Figure 12: Axial and circumferential profiles of DNT-2

3.4. Results

Based on the iterative analyses, the matched numerical dent profiles were obtained and shown in Figs. 13 and 14 for DNT-1 and DNT-2, respectively. Two (2) FE profiles were generated for each dent feature to capture the upper and lower bounds of the dent curvatures, i.e., FE Profile-1 and FE Profile-2.

https://doi.org/10.52202/078572-0069

The DFDI and SLD were calculated from failure strains defined in Eqs. (12) and (25), respectively, and summarized in Table 1. Surprisingly, PEEQ, SLD, and DFDI values from FE Profile-1 and Profile-2 are almost identical. That may be because the deformed curvatures near the dent apex are almost identical for both dents. The results of Table 1 also indicate that SLD values are generally less than DFDI values for a given dent feature, which is widely observed in the Level-3 dent assessment. The estimated DFDI values from the failure strain approach with scaling factor $b = 2.5$ are about 90.5% greater than those from the failure strain approach with scaling factor $b = 1.5$. It corresponds to the triaxiality ratio $\eta = 0.6 \sim 0.67$, as shown in Fig. 2, at the biaxial stress state. The estimated SLD values from Li & Xi's failure strain approach are about 27.5% greater than those from the ASME BPVC failure strain approach.

It is worth noting that the lower bound failure strains are defined differently in Eq. (12) and Eq. (25). The lower bound failure strain of DFDI is achieved by changing the scaling factor of stress triaxiality ratio, which means the difference in failure strain as well as DFDI will be exponentially more pronounced with the increase of stress triaxiality ratio. This reflects the theoretical and experimental observations, e.g., void volume grows easier in the biaxial stress state than in the uniaxial stress state. On the other hand, the lower bound failure strain of SLD is achieved by shifting the anchor point of the triaxial stress state, which is dependent on material properties and independent of the instantaneous stress triaxiality ratio (see Eq. (23)). Therefore, it may not be able to fully capture the reduction of failure strain at higher stress triaxiality ratios, which may limit its accuracy and applicability in dent ECA assessment. Therefore, it may be more appropriate to use DFDI for dent assessment rather than SLD based on the nature of their lower bound definitions.

In both cases, the maximum DFDI is about 0.9 from the scaling factor $b = 2.5$, which is close to the damage threshold. This could indicate an injurious dent if additional safety factors or other uncertainty factors are considered [4]. For example, the two incidents observed in the same line from the same manufacturer can indicate a unique case of void types, volume fractions, void distributions, 2nd phase particle, inclusion content, grain size, as well as material properties (e.g., strain hardening – m_2 of SLD's failure strain, elongation - m_3, m_4 of SLD's failure strain, and critical strain ε_0 of DFDI's failure strain). A higher volume fraction and/or the presence of a void cluster may accelerate the void growth and damage, which means a higher scaling factor may be more representative. A more systematic study on pipe steel is recommended for benchmarking the parameters in DFDI and SLD calculations.

It should be noted that the plastic strain is load-history dependent in nature, and the stress triaxiality ratio depends on the instantaneous loading condition. The stress and strain results from the iterative FE analyses may not represent the entire loading history of the dent investigated, where there might be a potential risk of underestimating the accumulated plastic strain. An additional safety factor should be considered based on engineering assessment best practices to mitigate it.

https://doi.org/10.52202/078572-0069

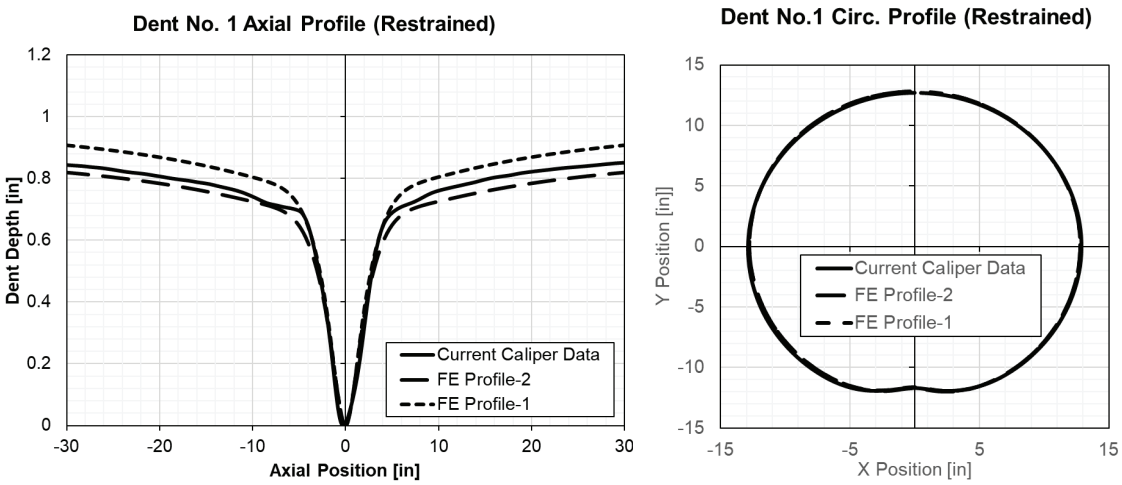

(a) Axial profile (b) Circumferential profile

Figure 13: Axial and circumferential profiles of DNT-1.

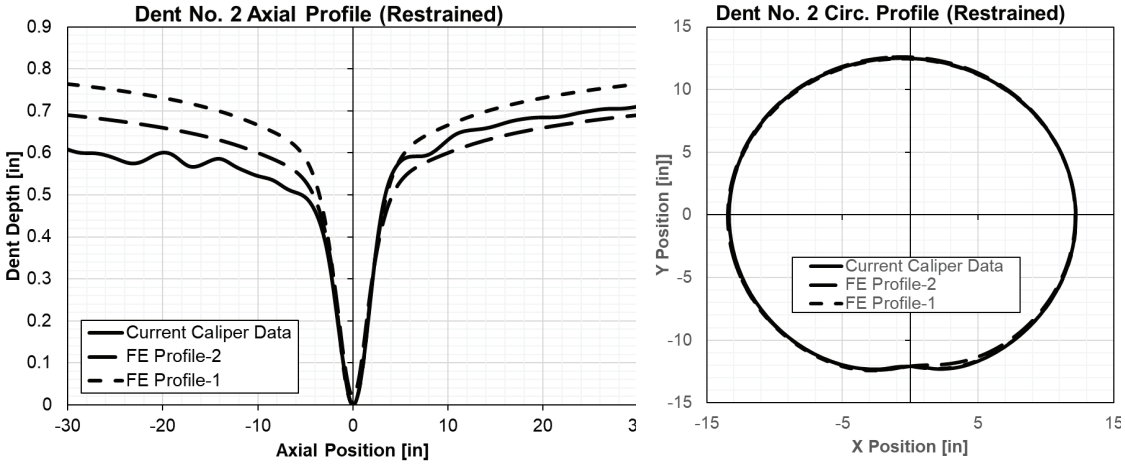

(a) Axial profile (b) Circumferential profile

Figure 14: Axial and circumferential profiles of DNT-2.

Table 1: PEEQ, DFDI and SLD results.

DNT #	FE Profile #	DFDI		SLD		PEEQ
		$\varepsilon_{f,b=1.5}$	$\varepsilon_{f,b=2.5}$	ASME BPVC	Li & Xi	
DNT-1	Profile-1	0.50	0.93	0.40	0.51	9.7%
	Profile-2	0.50	0.93	0.40	0.51	9.7%
DNT-2	Profile-1	0.47	0.90	0.38	0.48	8.9%
	Profile-2	0.47	0.90	0.38	0.48	8.9%

https://doi.org/10.52202/078572-0069

4. Conclusion Remarks and Recommendations

This study systematically reviewed the failure strain approaches used in DFDI and SLD assessments, and the recent developments were also summarized. For DFDI's failure strain, a lower bound approach was proposed in [6] using a stress triaxiality scaling factor of 2.5 instead of 1.5 in the formulation. The revised scaling factor was introduced by capturing the void interactions at different stress triaxiality ratios. It was also found that void interactions can accelerate the reduction of failure strains. For SLD's failure strain, a lower bound approach was developed in [25] by shifting the stress triaxiality ratio from the uniaxial state to the worst-case state that is interpreted as a function of material properties using the same parameters in ASME BPVC. The lower bound failure strain approach can reduce the non-conservatism in DFDI or SLD calculations.

The study also included two dents that interact with metal loss and cracks. The cracks were identified from the field assessment but failed to be identified in the past dent ECA assessment. The Level-3 FE assessments on two dents were conducted again, and both conventional and revised failure strain approaches were used in the DFDI and SLD calculations. After iterative FE studies, the numerical dent profiles match those from the calliper data. The maximum PEEQ values are about 9 ~ 10%, and the maximum DFDI and SLD values from the revised failure strain approaches are about 0.9, which can be regarded as an injured dent if considering the safety factor and other uncertainty factors. In addition, it was found that the revised DFDI's failure strain with a scaling factor of 2.5 can capture the exponential relationship between the stress triaxiality ratio and failure strain, but the revised SLD's failure strain with a shifting anchor point of the stress triaxiality ratio may not. The differences between DFDI's and SLD's approaches may be more pronounced if the void interaction becomes the predominant local failure mechanism, or the stress state is close to the biaxial stress state.

The following practices are recommended for the DFDI and SLD evaluations:

(1) For DFDI calculations, Eq. (12) is recommended for the failure strain evaluation, which includes upper bound (conventional) and lower bound (revised) scenarios. Note that the upper and lower bound failure strains refer to lower and upper bound DFDI/SLD values, respectively.

(2) For SLD calculations, Eq. (25) is recommended for the failure strain evaluation, which includes upper bound (conventional) and lower bound (revised) scenarios.

(3) The engineering decision should be made by considering the maximum DFDI or SLD from Eq. (12) or Eq. (25). The DFDI and SLD from lower bound failure strains should be used as the upper bound reference values if limited material information is provided (e.g., type or size of void, presence of void cluster, void volume fraction, 2nd phase particle, inclusion content, grain size).

(4) The revised DFDI approach (Eq. 12) is recommended in dent ECAs.

https://doi.org/10.52202/078572-0069

(5) The revised SLD approach (Eq. 25) with both upper and lower bounds is better than the present approach employed in API 1183.

(6) Further experimental and numerical studies on pipeline steel are recommended for calibrating failure strain-related parameters.

5. References

[1] R. Y. Wang, R. Kania, U. Arumugam, and M. Gao, "A Combined Approach to Characterization of Dent With Metal Loss," in Volume 2: Pipeline Integrity Management, Calgary, Alberta, Canada: American Society of Mechanical Engineers, Sep. 2012, pp. 209–216. doi: 10.1115/IPC2012-90499.

[2] M. Gao, R. Krishnamurthy, S. Tandon, and U. Arumugam, "Critical Strain Based Ductile Damage Criterion and its Application to Mechanical Damage in Pipelines".

[3] U. Arumugam, M. Gao, R. Krishnamurthy, R. Wang, and R. Kania, "Root Cause Analysis of Dent With Crack: A Case Study," doi: 10.1115/IPC2012-90504.

[4] R. Wang and K. Zhang, "Gaps in the Current Strain-Based Dent Assessment," in Volume 2: Pipeline and Facilities Integrity, Calgary, Alberta, Canada: American Society of Mechanical Engineers, Sep. 2022, p. V002T03A032. doi: 10.1115/IPC2022-87165.

[5] S. Wu, J. Bratton, J. Wang, D. Kemp, L. Xu, and G. Quickel, "To Dig or Not to Dig – Determining Which Dents are Suitable for Engineering Critical Assessment per 192.712 (c)," presented at the 2024 PPIM Conference, Accessed: Jan. 03, 2025. [Online]. Available: https://ppimconference.com/2024-conference-program/

[6] D. Chae and D. A. Koss, "Damage accumulation and failure of HSLA-100 steel," Materials Science and Engineering: A, vol. 366, no. 2, pp. 299–309, Feb. 2004, doi: 10.1016/j.msea.2003.08.040.

[7] J. R. Rice and D. M. Tracey, "On the ductile enlargement of voids in triaxial stress fields∗," Journal of the Mechanics and Physics of Solids, vol. 17, no. 3, pp. 201–217, Jun. 1969, doi: 10.1016/0022-5096(69)90033-7.

[8] T. Yamada and Ohata, Mitsuru, "Application of damage model based on void growth analysis to ductile crack growth simulation," Welding International, vol. 33, no. 1–3, pp. 30–41, 2019, doi: 10.1080/09507116.2020.1864997.

[9] F. A. McClintock, "A Criterion for Ductile Fracture by the Growth of Holes," Journal of Applied Mechanics, vol. 35, no. 2, pp. 363–371, Jun. 1968, doi: 10.1115/1.3601204.

[10] G. R. Johnson and W. H. Cook, "Fracture characteristics of three metals subjected to various strains, strain rates, temperatures and pressures," Engineering Fracture Mechanics, vol. 21, no. 1, pp. 31–48, Jan. 1985, doi: 10.1016/0013-7944(85)90052-9.

[11] V. Tvergaard and A. Needleman, "Analysis of the cup-cone fracture in a round tensile bar," Acta Metallurgica, vol. 32, no. 1, pp. 157–169, Jan. 1984, doi: 10.1016/0001-6160(84)90213-X.

[12] J. C. Sowinski, "ASME Section VIII – Division 2 Criteria and Commentary," 2014.

https://doi.org/10.52202/078572-0069

[13] API RP 1183: Assessment and Management of Dents in Pipelines.

[14] J. W. Hancock and A. C. Mackenzie, "On the mechanisms of ductile failure in high-strength steels subjected to multi-axial stress-states," Journal of the Mechanics and Physics of Solids, vol. 24, no. 2, pp. 147–160, Jun. 1976, doi: 10.1016/0022-5096(76)90024-7.

[15] F. D. Fischer, O. Kolednik, G. X. Shan, and F. G. Rammerstorfer, "A note on calibration of ductile failure damage indicators," Int J Fract, vol. 73, no. 4, pp. 345–357, 1995, doi: 10.1007/BF00027274.

[16] Y. Huang, "Accurate Dilatation Rates for Spherical Voids in Triaxial Stress Fields," Journal of Applied Mechanics, vol. 58, no. 4, pp. 1084–1086, Dec. 1991, doi: 10.1115/1.2897686.

[17] L. Xue, "Ductile fracture modeling : theory, experimental investigation and numerical verification," Thesis, Massachusetts Institute of Technology, 2007. Accessed: Dec. 28, 2024. [Online]. Available: https://dspace.mit.edu/handle/1721.1/40876

[18] T. Wierzbicki and L. Xue, "Lab Report 136 original version: On the Effect of the Third Invariant of the Stress Deviator on Ductile Fracture," 2024, doi: 10.13140/RG.2.2.15446.83528.

[19] I. Barsoum and J. Faleskog, "Rupture mechanisms in combined tension and shear—Experiments," International Journal of Solids and Structures, vol. 44, no. 6, pp. 1768–1786, Mar. 2007, doi: 10.1016/j.ijsolstr.2006.09.031.

[20] M. Dunand and D. Mohr, "On the predictive capabilities of the shear modified Gurson and the modified Mohr–Coulomb fracture models over a wide range of stress triaxialities and Lode angles," Journal of the Mechanics and Physics of Solids, vol. 59, no. 7, pp. 1374–1394, Jul. 2011, doi: 10.1016/j.jmps.2011.04.006.

[21] T. Wierzbicki, Y. Bao, Y.-W. Lee, and Y. Bai, "Calibration and evaluation of seven fracture models," International Journal of Mechanical Sciences, vol. 47, no. 4, pp. 719–743, Apr. 2005, doi: 10.1016/j.ijmecsci.2005.03.003.

[22] Y. Bao and T. Wierzbicki, "On fracture locus in the equivalent strain and stress triaxiality space," International Journal of Mechanical Sciences, vol. 46, no. 1, pp. 81–98, Jan. 2004, doi: 10.1016/j.ijmecsci.2004.02.006.

[23] API, "API Specification 5L, 46 ed.," 2019. doi: 10.1590/s1413-73722008000100023.

[24] ASTM, "E8/E8M — 16a Standard Test Methods for Tension Testing of Metallic Materials 1," 2018, doi: 10.1520/E0008_E0008M-16A.

[25] X.-X. (Lambert) Li and F. Xi, "Strain Limits Against Local Fracture of Vessels and Components," presented at the ASME 2020 Pressure Vessels & Piping Conference, American Society of Mechanical Engineers Digital Collection, Oct. 2020. doi: 10.1115/PVP2020-21028.

[26] API 579: Standard: Fitness For Service Assessment Procedure.

[27] API 5L: Line Pipe.